Minimal Surfaces: A Three Dimensional Segmentation Approach

Vicent Caselles *
Ron Kimmel †
Guillermo Sapiro ‡
Catalina Sbert §

Abstract

A novel geometric approach for three dimensional object segmentation is presented. The scheme is based on geometric deformable surfaces moving towards the objects to be detected. We show that this model is equivalent to the computation of surfaces of minimal area (local minimal surfaces) in a Riemannian space. This space is defined by a metric induced from the three dimensional image in which the objects are to be detected. The model also shows the relation between classical deformable surfaces obtained via energy minimization, and geometric ones derived from curvature flows in the surface evolution framework. The new approach is stable, robust, and automatically handles changes in the surface topology during the deformation. Results related to existence, uniqueness, stability, and correctness of the solution to this geometric deformable model are presented as well. Based on an efficient numerical algorithm for surface evolution, we present a number of examples of object detection in real and synthetic images.

Key words: 3D object segmentation, dynamic surfaces, variational problems, differential geometry, Riemannian geometry, minimal surfaces, topology free boundary detection.

*Dept. of Mathematics and Informatics, University of Illes Balears, 07071 Palma de Mallorca, Spain, dmivca0@ps.uib.es
†Dept. of Electrical Engineering, Technion, I.I.T., Haifa 32000, Israel, ron@tx.technion.ac.il
‡Hewlett-Packard Labs, 1501 Page Mill Road, Palo Alto, CA 94304, guille@hpl.hp.com
§Dept. of Mathematics and Informatics, University of Illes Balears, 07071 Palma de Mallorca, Spain,

1 Introduction

One of the basic problems in image analysis is object detection. This can be associated with the problem of boundary detection, when boundary is roughly defined as a curve or surface separating homogeneous regions. "Snakes," or active contours, were proposed by Kass *et al.* [23] to solve this problem, and received a great deal of attention from the image analysis community since then. The work was later extended to 3D surfaces. The classical snakes and 3D deformable surfaces approach, reviewed in the following section, are based on deforming an initial contour or surface towards the boundary of the object to be detected. The deformation is obtained by trying to minimize a functional designed such that its (local) minima is obtained at the boundary of the object. These active surfaces are examples of the general technique of matching deformable models to image data by means of energy minimization [5, 55]. The energy is basically composed by a term which controls the smoothness of the surface and another one that attracts it to the boundary. This energy model is not capable of changing its topology when direct implementations are performed. The topology of the final surface will be in general as that of the initial one, unless special procedures are implemented for detecting possible splitting and merging points [36, 53]. This may be a problem when an un-known number of objects must be simultaneously detected. This approach is also non intrinsic, i.e., the energy functional depends on the parametrization. See for example [34] for comments on advantages as well as disadvantages of energy approaches for deforming contours.

Recently, geometric models of deformable contours/surfaces were simultaneously proposed by Caselles *et al.* [6] and by Malladi *et al.* [33, 34, 35], and are also reviewed in the following section. These models are based on the theory of surface evolution and geometric flows, which has gained a large amount of attention from the image analysis community in the past years [2, 3, 19, 25, 27, 28, 30, 31, 32, 45, 46, 47, 48, 49, 50]. In these models, the curve/surface is propagating (deforming) by an implicit velocity that also contains two terms, one related to the regularity of the deforming shape and the other attracting it to the boundary. The model is given by a geometric flow (PDE), based on mean curvature motion, and not by an energy function. This model allows automatic changes in topology when implemented using the level-sets numerical algorithm [40]. Thereby, several objects can be detected simultaneously, without previous knowledge of their exact number in the scene, and without special tracking procedures.

In [7], we showed the relation between these two approaches for two dimensional object detection (two dimensional curve evolution), proposing what we called "geodesic active contours." We first proved that, for a particular case, the classical energy approach is equivalent to finding a geodesic curve in a Riemannian space with a metric derived from the image. This means that the boundary we are looking for is the path of minimal distance, measured in the Riemannian metric, that connects two given image points. We then showed that assuming a level set representation of the deforming contour, we can find this geodesic curve via a geometric flow which is very similar to the one obtained in the curve evolution approaches mentioned above. This flow, however, includes a new term that improves those models. [1]

[1] Although this term appears in similar forms in classical snakes, it was missing in curve evolution models. This term is naturally incorporated by the geodesic formulation.

The new term allows to track, in an accurate way, boundaries with high variation in their gradient, a task that was impossible with previous curve evolution models. We also showed that the solution of the flow exists in the viscosity framework, and is unique and stable. Therefore, the approach presented in [7] has the following main properties: 1- Connects energy and curve evolution approaches of active contours. 2- Presents the snake problem as a geodesic computation one. 3- Improves existing models as a result of the geodesic formulation. 4- Allows simultaneous detection of interior and exterior boundaries in several objects without special contour tracking procedures. 5- Holds formal existence, uniqueness, and stability results. 6- Stops automatically.

In this paper we extend the results in [7] to three dimensional object detection. The obtained geometric flow is based on geometric deformable surfaces. We show that the desired boundary is given by a minimal surface in a Riemannian space defined by the image. Therefore, segmentation is achieved via the computation of surfaces of minimal area, where the area is defined in a non-Euclidean space. The obtained flow has the same advantages over other 3D deformable models as the advantages of the geodesic active contours over previous 2D approaches.

This paper is organized as follows. In Section 2 we briefly review both classical energy based and surface evolution based deformable models. In Section 3 we describe the main results on 2D geodesic active contours as presented in [7], which will help us to develop the 3D minimal surface deformable models, presented in Section 4. Results concerning existence and uniqueness of the proposed model are given in Section 5, and those related to its correctness in Section 6. Experimental results are given in Section 7 and concluding remarks in Section 8.

2 Basic approaches on snakes and deformable shapes

2.1 Energy based snakes

We start with a description of classical energy snakes, first for 2D objects and then for 3D ones.

Let $\mathcal{C}(p) : [0,1] \rightarrow I\!R^2$ be a parametrized planar curve, and $I : [0,a] \times [0,b] \rightarrow I\!R^+$ a given image where we want to detect the objects boundaries. The classical snakes approach [23] associates to the curve $\mathcal{C}$ an energy given by

$$E(\mathcal{C}) = \alpha \int_0^1 |\mathcal{C}'(\tau)|^2 d\tau + \beta \int_0^1 |\mathcal{C}''(\tau)|^2 d\tau - \lambda \int_0^1 |\nabla I(\mathcal{C}(\tau))| d\tau, \tag{1}$$

where α, β, and λ are real positive constants (α and β impose the elasticity and rigidity of the curve). The first two terms basically control the smoothness of the contours to be detected (internal energy), [2] while the third term is responsible for attracting the contour towards the object in the image (external energy). Solving the problem of snakes amounts to finding, for a given set of constants α, β, and λ, the curve $\mathcal{C}$ that minimizes E. As argued in Caselles *et al.* [6], the snake method provides an accurate location of the edges near a given initialization of the curve and it is capable to extract smooth shapes. They also showed that

[2] Other smoothing constraints can be used, being this the most common one.

the snakes model can retrieve angles for all values of parameters α, $\beta \geq 0$ $(\alpha+\beta>0)$. This is, in some sense, related to the adaptation of the set of parameters α, β to the problem in hand. On the other hand, it does not directly allows simultaneous treatment of several contours. Note that when considering more than one object in the image, and for example the initial prediction of $\mathcal{C}$ surrounds all of them, it is not possible to detect all the objects. In other words, the classical (energy) approach of the snakes can not deal with changes in topology, unless special topology handling procedures are added [36]. The topology of the initial curve will be the same as the one of the (possible wrong) final solution. The geometric models in [6, 7, 33, 34, 35] automatically overcome this problem.

It is clear that the classical snake method can be generalized to 3D data images, where the boundaries of the objects are surfaces. This extension is known as the deformable surface model, and was introduced by Terzopoulos *et al.* [55] for a 3D representation of objects and extended and used for a 3D segmentation by many others (see for example [11, 12, 13]). In the 3D case, a parametrized surface

$$v(r,s)=(x(r,s),y(r,s),z(r,s)) \qquad (r,s)\in[0,1]\times[0,1]$$

is considered, and the energy functional is given by

$$E(v)=\int_\Omega \left[\omega_{10}\left|\frac{\partial v}{\partial r}\right|^2+\omega_{01}\left|\frac{\partial v}{\partial s}\right|^2+2\omega_{11}\left|\frac{\partial^2 v}{\partial r\partial s}\right|^2+\omega_{20}\left|\frac{\partial^2 v}{\partial r^2}\right|^2+\omega_{02}\left|\frac{\partial^2 v}{\partial s^2}\right|^2+P(v(r,s))\right]drds, \tag{2}$$

where $P:=-\parallel \nabla I \parallel^2$, or any related decreasing function of the gradient. Like the 2D case, the algorithm starts with an initial surface $\mathcal{S}_0$, generally near the desired 3D boundary O, and tries to move $\mathcal{S}_0$ towards a local minimum of E.

These are the basic formulations of the 2D and 3D snakes. Other related formulations have been proposed in the literature. Reviewing all of them is out of the scope of this paper.

2.2 Deformable models based on mean curvature motion

Recently, novel geometric models of deformable curves were simultaneously proposed by Caselles *et al.* [6] and by Malladi *et al.* [33, 34, 35]. Assume in the 2D case that the deforming curve $\mathcal{C}$ is given as a level-set of a function $u:\mathbb{R}^2\to\mathbb{R}$. Then, we can represent the deformation of $\mathcal{C}$ via the deformation of u. In this case, the proposed 2D deformation is given by

$$\frac{\partial u}{\partial t} = g(I)|\nabla u|\mathrm{div}\left(\frac{\nabla u}{|\nabla u|}\right)+\nu g(I)|\nabla u| \qquad (t,x)\in[0,\infty[\times\mathbb{R}^2 \tag{3}$$

$$u(0,x) = u_0(x) \qquad x\in\mathbb{R}^2 \tag{4}$$

where ν is a positive real constant,

$$g(I)=\frac{1}{1+|\nabla\hat{I}|^p}, \tag{5}$$

$\hat{I}$ being a regularized version of the original image I where we are looking for the contour of an object O and $p=1$ or 2. Typically, the initial condition $u(0,x)=u_0(x)$, in the case of outer snakes (curves evolving towards the boundary of O from the exterior of O), was taken as a regularized version of $1-\chi_C$ where χ_C is the characteristic function of a set $\mathcal{C}$ containing O. Using the fact that

$$\operatorname{div}\left(\frac{\nabla u}{|\nabla u|}\right)=\kappa,$$

where κ is the Euclidean curvature [22] of the level sets $\mathcal{C}$ of u Equation (3) can be written in the form

$$u_t = g(I)(\nu+\kappa)|\nabla u|.$$

Equation (3) can be interpreted as follows: Suppose that we are interested in following a certain level set of u, which, to fix ideas, we suppose to be the zero level set. Suppose also that this level set is a smooth curve. Then the flow

$$u_t = (\nu+\kappa)|\nabla u|,$$

means that the the level set $\mathcal{C}$ of u we are considering is evolving according to

$$\mathcal{C}_t = (\nu+\kappa)\vec{\mathcal{N}}, \tag{6}$$

where $\vec{\mathcal{N}}$ is the inward normal to the curve. [3] This equation was first proposed in [40, 54], were extensive numerical research on it was performed. It was recently introduced in [25] for shape analysis. The motion

$$\mathcal{C}_t = \kappa\vec{\mathcal{N}},$$

denoted as *Euclidean heat flow* is very well know for its excellent geometric smoothing properties [4, 20, 21]. (This flow was extended in [46, 47, 48] for the affine group and in [38, 48] for others.) This flow is also called the *Euclidean shortening flow*, since it moves the curve in the gradient direction of the length functional given by

$$L := \oint_{\mathcal{C}} ds, \tag{7}$$

where $ds = |\mathcal{C}_p|dp$ is the Euclidean arc-length element. Therefore, this flow decreases the length of the curve as fast as possible. This property is important for the geometric interpretation of the geodesic and minimal surface models that are developed in this paper.

The constant velocity $\nu\vec{\mathcal{N}}$ in (6), which is related with classical mathematical morphology [45] and shape offsetting in CAD [26], acts as the balloon force in [12]. Actually this velocity pushes the curve inwards and it is crucial in the model in order to allow convex initial curves to become non-convex, and thereby detect non-convex objects. [4] Of course, the ν parameter must be specified a priori in order to make the object detection algorithm automatic. This is not a trivial issue, as pointed out in [6], where possible ways of estimating this parameter are considered. In [6] the authors also present existence and uniqueness results (in the viscosity

[3] Based on the fact that $\vec{\mathcal{N}} \parallel \nabla u$, it is straightforward to prove that when the level sets $\mathcal{C}$ of u evolve according to $\mathcal{C}_t = \beta\vec{\mathcal{N}}$, the function u deforms via $u_t = \beta|\nabla u|$.

[4] A convex curve remains convex when evolving according to the Euclidean heat flow [20].

framework) of the solutions of (3). Recapping, the "force" $(\nu+\kappa)$ acts as the internal force in the classical energy based snakes model. The external force is given by $g(I)$, which is supposed to prevent the propagating curve from penetrating into the objects in the image. In [6, 33, 34, 35], the authors choose $g(I)$ given by (5). $\hat{I}$ was smoothed using Gaussian filtering, but more effective geometric smoothers, as those in [3, 50], can be used as well. Note that other decreasing functions of the gradient may be selected as well. For an ideal edge, $\nabla\hat{I}=\delta$, $g=0$, and the curve stops at the edge ($u_t=0$). The boundary is then given by the set $u=0$.

This curve evolution model given by (3) automatically handles different topologies. That is, there is no need to know a priori the topology of the solution. This allows to detect any number of objects in the image, without knowing their exact number. This is achieved with the help of an efficient numerical algorithm for curve evolution, developed by Osher and Sethian [40, 54], and used by others for different image analysis problems [10, 25, 27, 30, 31, 45, 47, 49], and analyzed for example in [9, 18]. In this case, the topology changes are automatically handled, without the necessity for specific monitoring the topology of the deforming curve.

The model (3) can easily be extended to 3D object detection. Let us consider for each $t\geq 0$ a 3D function $u(t,.):I\!R^3\rightarrow I\!R$, and denote by $\mathcal{S}$ its level-sets (3D surfaces). Then the 3D geometric deformable model is given by:

$$\begin{aligned}\frac{\partial u}{\partial t} &= g(I)|\nabla u|\operatorname{div}\left(\frac{\nabla u}{|\nabla u|}\right)+\nu g(I)|\nabla u| \\ &= g(I)(\nu+\mathbf{H})|\nabla u|,\end{aligned} \tag{8}$$

where now $\mathbf{H}$ is the sum of the two principal curvatures of the level sets $\mathcal{S}$, that is, twice its mean curvature. This model has the same concepts as the 2D one, and is composed by three elements:

1. A smoothing term. In the case of (8), this smoothing term $\mathbf{H}$ is twice the mean curvature, but other more efficient smoothing velocities as those proposed in [2, 8, 39] can be used. [5]

2. A constant balloon-type force ($\nu|\nabla u|$).

3. A stopping factor ($g(I)$).

The goal of this paper is to extend this model, motivated by the extension of (3) to the geodesic active contours as was done in [7] and reviewed in next section.

3 Geodesic active contours

We now review the main results of [7]. Let us consider a particular case of (1), where $\beta=0$. Two main reasons motivate this selections: First, this will allow us to derive the relation

[5] Although curvature flows smooth curves in 2D [21, 46, 47], no curvature flow that smoothes all possible surfaces was yet found in 3D [39]. Frequently used flows are mean curvature or positive part of Gaussian curvature flows [2, 8].

between energy based active contours and geometric curve evolution ones. Second, although having $\beta \neq 0$ adds flexibility and other properties, the regularization effect on the geodesic active contours comes from curvature based curve flows, obtained only from the other terms in (1). This allows to achieve smooth curves in the proposed approach without having the high order derivatives given by $\beta \neq 0$. The use of the curvature driven curve motions for smoothing was proved to be very efficient in previous works [2, 6, 25, 34, 42, 47], and is also supported by our experiments in [7] and Section 7. Therefore, curve smoothing will be obtained also with $\beta = 0$, keeping only the first regularization term. Assuming this, and replacing the edge detector $|\nabla I|$ by a general function $g(|\nabla I|)^2$ of the gradient such that $g(r) \to 0$ as $r \to \infty$, we obtain,

$$E(\mathcal{C}) = \alpha \int_0^1 |\mathcal{C}'(\tau)|^2 d\tau + \lambda \int_0^1 g(|\nabla I(\mathcal{C}(\tau))|)^2 d\tau = E_{int}(\mathcal{C}) + E_{ext}(\mathcal{C}). \tag{9}$$

(In order to simplify the notation, we will sometimes write $g(I)$ or $g(\mathcal{X})$ ($\mathcal{X} \in I\!R^2$) instead of $g(|\nabla I|)$.) The goal now is to minimize E in (9) for $\mathcal{C}$ in a certain allowed space of curves. Of course, in (9), only the ratio λ/α counts.

As argued in [7], the functional (9) is not intrinsic, i.e., it depends on the parametrization of the curve. This could be considered as an undesirable property since parametrizations are not related to the geometry of the curve (or object boundary), but only to the velocity they are traveled. Motivated by the discussion on ideal edges, in [7], we proposed to fix this degree of freedom by fixing the energy level $E_0 = 0$ at the local minima (other values are analyzed in [7] as well). Then with the help of Maupertuis' Principle [17], we proved that the solution of (9) is given by a geodesic curve in a Riemannian space. The metric in this Riemannian space is defined by $g_{ij}\, dx_i dx_j$ with $g_{ij} = g(I)^2 \delta_{ij}$. This means that the object is detected when a curve of minimal length is found. In other words, we proved that minimizing (9) is equivalent to solving

$$\mathrm{Min}_{\mathcal{C}} \int_0^1 g(|\nabla I(\mathcal{C}(\tau)|)|\mathcal{C}'(\tau)| d\tau. \tag{10}$$

We have transformed the problem into a problem of geodesic computation in a Riemannian space, according to a new metric (length measure) given by

$$L_R := \int_0^1 g(|\nabla I(\mathcal{C}(\tau)|)|\mathcal{C}'(\tau)| d\tau. \tag{11}$$

Since $|\mathcal{C}'(\tau)| d\tau = ds$, we may write

$$L_R := \int_0^L g(|\nabla I(\mathcal{C}(\tau)|) ds.$$

where L denotes the Euclidean length of $\mathcal{C}(\tau)$. Comparing this with the classical Euclidean length as given in previous section by (7), we find that the new length is obtained by weighting ds with $g(|\nabla I(\mathcal{C}(\tau)|)$, which contains information regarding the boundary of the object. Therefore, when trying to detect an object, we are not just interested in finding the path of minimal classical length ($\oint ds$) but the one which minimizes a new definition of length which takes into account image characteristics. Note that (10) is general, no assumptions on

g were done, besides being a decreasing function. Therefore, the theory of detection based on geodesic computations given above, and fully described in [7], is general.

In order to find this geodesic curve, we use the steepest descent method which will give us a local minima of (11). The, the flow minimizing L_R is given by [7]

$$\mathcal{C}_t = (g\kappa - \nabla g \cdot \vec{\mathcal{N}})\vec{\mathcal{N}} \tag{12}$$

To introduce the level set formulation, let us assume that a curve $\mathcal{C}$ is parametrized as a level set of a function $u : [0, a] \times [0, b] \rightarrow I\!R$. That is, $\mathcal{C}$ is such that it coincides with the set of points in u such that $u =$ constant. (In our case we choose the curve to be represented by the set $u = 0$.) In particular given an initial curve $\mathcal{C}_0$ we parametrize it as a zero level set of a function u_0. Then, the level set formulation of the steepest descent method says that solving the above geodesic problem starting from $\mathcal{C}_0$ amounts to searching for the steady state ($\frac{\partial u}{\partial t} = 0$) of the following evolution equation:

$$\begin{aligned} \frac{\partial u}{\partial t} &= |\nabla u| \mathrm{div}\left(g(I)\frac{\nabla u}{|\nabla u|}\right) && (13) \\ &= g(I)|\nabla u| \mathrm{div}\left(\frac{\nabla u}{|\nabla u|}\right) + \nabla g(I) \cdot \nabla u, && (14) \end{aligned}$$

with initial datum $u(0, x) = u_0(x)$. This equation is then obtained by computing the gradient descent of L_R and embedding the flow as the level set of u. We have obtained the main part of the novel active contour model we propose.

Comparing Equation (13) to (3), we see that the term $\nabla g \cdot \nabla u$ is missing in the old model. This is due the fact that in (3), a classical length in Euclidean space is used (given by (7)). In the new model, the length takes into account the image structure, and is given by (11), defining a new Riemannian space. This new term directs the curve towards the boundary of the objects ($-\nabla g$ points toward the center of the boundary). Observe the $2D$ case of an image I of an object of high intensity value and low intensity background. Figure 1 shows I (top-left) and its smoothed version $\hat{I}$ (top-right). The function g is shown in the bottom, together with its gradient vectors. Observe the way the gradient vectors are all directed towards the middle of the boundary. Those vectors direct the propagating curve into the valley of the g function. In this $2D$ case, $\nabla g \cdot \vec{\mathcal{N}}$ is effective in case the gradient vectors coincide with normal direction of the propagating curve. Otherwise, it will lead the propagating curve into the boundary and eventually force it to stay there. Recapping, this new force increases the attraction of the deforming contour towards the boundary, being of special help when the boundary has high variations of its gradient values. Note that in the old model, the curve stops when $g = 0$. This happens only, along an ideal edge. Also, if there are different gradient values along the edge, as it often happens in real images, then g gets different values at different locations along the object boundaries. It is necessary to consider all those values as high enough to guarantee the stopping of the propagating curve. This makes the geometric model (3) inappropriate for the detection of boundaries with (unknown) high variations of the boundary gradients. In our new model, the curve is attracted to the boundary also by the new term (note again that the gradient vectors point towards the middle of the boundary, Figure 1). Thereby, it is also possible to detect boundaries with

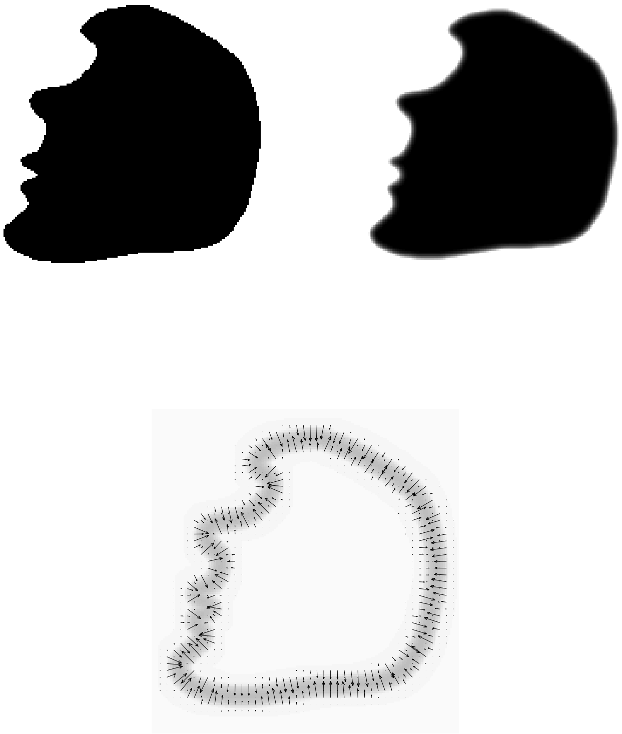

Figure 1: Geometric interpretation of the new term in the proposed deformable model. The gradient vectors are all directed towards the middle of the boundary. Those vectors direct the propagating curve into the valley of the g function.

high differences in their gradient values. The second advantage of this new term is that we remove the necessity of the constant velocity given by ν. This constant velocity, that mainly allows the detection of non-convex objects, introduces an extra parameter to the model, that in most cases is an undesirable property. In our case, the new term allows the detection of non-convex objects as well. This term also helps when starting from curves inside the object. In case we wish to add this constant velocity, in order for example to increase the speed of convergence, we can just consider the term $\nu g(I)|\nabla u|$ as an extra speed in the geodesic problem (10), obtaining

$$\frac{\partial u}{\partial t} = |\nabla u| \mathrm{div} \left(g(I) \frac{\nabla u}{|\nabla u|} \right) + \nu g(I)|\nabla u|. \tag{15}$$

This equation is of course equivalent to

$$\frac{\partial u}{\partial t} = g(\nu + \kappa)|\nabla u| + \nabla u \cdot \nabla g. \tag{16}$$

Equation (15), which is the solution of the geodesic problem (10) with an extra speed, constitutes the *geodesic active contour* model we propose. [6] As shown in the examples in [7], it is possible to choose $\nu = 0$ (no constant velocity), and the model still converges to the correct solution (in a slower motion). The advantage is that we have obtained a model with less parameters.

Existence, uniqueness and stability results for the geodesic active contour model, Equation (15), were stated in [7]. Analogous results will be stated below (see Section 5) for the corresponding 3D extension which we introduce in the next Section.

4 Three dimensional deformable models as minimal surfaces

In the previous section, we presented a model for 2D object detection based on the computation of geodesics in a given Riemannian space. This means that we are computing paths or curves of minimal (weighted) length. This extends to 3D surfaces by computing surfaces of minimal area, where area is defined in a given Riemannian space as well. In the 2D case, length is given by (7), and the new length which allows to perform object detection is given by (11). In the case of surfaces, (7) is replaced by area

$$A := \int\int da, \tag{17}$$

and (11) by "weighted" area

$$A_R := \int\int g(I) da, \tag{18}$$

[6] Related equations were recently independently proposed by Kichenassamy *et al.* [24] and by Shah [52], based on a different approach.

where da is the (Euclidean) element of area. [7] Surfaces minimizing (17) are denoted as *minimal surfaces* [41]. In the same way, we will denote by minimal surfaces these surfaces that minimize (18). The difference between A and A_R is like the difference between L and L_R, and is given by the metric. In A, the element of area is given by the classical element da in Euclidean space, while in A_R, the area element da_r is given by $g(I)da$. Observe that this area element corresponds to the area element induced on a surface of $I\!R^3$ by the metric of $I\!R^3$ given by $g_{ij}\,dx_i dx_j$ with $g_{ij} = g(I)^2\delta_{ij}$. This is the 3D analogue of the metric used in [7] to construct the geodesic active contour model (see (11)). The basic element of our deformable model will be given by minimizing (18) by means of an evolution equation obtained from its Euler-Lagrange. Given the definition of A_R above, the computations are straightforward and are direct extension of the geodesic active contours computation as presented in the previous section and in [7]. We will point out only the basic characteristics of this flow.

The Euler-Lagrange of A is given by the mean curvature $\mathbf{H}$, obtaining a curvature flow

$$\frac{\partial \mathcal{S}}{\partial t} = \mathbf{H}\vec{\mathcal{N}}, \tag{19}$$

where $\mathcal{S}$ is the 3D surface and $\vec{\mathcal{N}}$ its inner unit normal. In a level sets notation, if for each $t \geq 0$, the evolving surface $\mathcal{S}$ is the zero level set of a function $u(t,.) : I\!R^3 \to I\!R$, which we take negative inside $\mathcal{S}$ and positive outside, we obtain the equation

$$u_t = |\nabla u| \mathrm{div}\left(\frac{\nabla u}{|\nabla u|}\right) = |\nabla u|\mathbf{H}. \tag{20}$$

Therefore, the mean curvature motion provides a flow that computes (local) minimal surfaces [10].

Computing now the Euler-Lagrange of A_R, we get

$$\mathcal{S}_t = (g\mathbf{H} - \nabla g \cdot \vec{\mathcal{N}})\vec{\mathcal{N}}. \tag{21}$$

This is the basic weighted minimal surface flow. Taking a level set representation, in analogy with (13), the steepest descent method to minimize (18) gives

$$\begin{aligned} \frac{\partial u}{\partial t} &= |\nabla u| \mathrm{div}\left(g(I)\frac{\nabla u}{|\nabla u|}\right) \\ &= g(I)|\nabla u| \mathrm{div}\left(\frac{\nabla u}{|\nabla u|}\right) + \nabla g(I) \cdot \nabla u. \end{aligned} \tag{22}$$

However, now u is a 4D function with $\mathcal{S}$ its 3D zero level set. We note again that comparing with previous surface evolution approaches for 3D object detection, the minimal surfaces model includes a new term, $\nabla g \cdot \nabla u$.

As in the 2D case, we can add a constant force to the minimization problem, obtaining the general *minimal surfaces model* for object detection:

$$\frac{\partial u}{\partial t} = |\nabla u| \mathrm{div}\left(g(I)\frac{\nabla u}{|\nabla u|}\right) + \nu g(I)|\nabla u|. \tag{23}$$

[7] In the same way as minimizing L_R is equivalent to minimizing (9), minimizing A_R is equivalent to minimizing the analogue 3D energy obtained from (2).

This is the flow we will further analyze and use for 3D object detection. It has the same properties and geometric characteristics as the geodesic active contours, leading to accurate numerical implementations and topology free object segmentation.

In [14] it was shown that the maximum curvature magnitude along the geodesics minimizing L_R given by Equation (11) is given by

$$\max\{|\kappa|\} = \sup_{\tau\in[0,1]} \left\{ \frac{|\nabla g(\mathcal{C}(\tau)) \cdot \vec{\mathcal{N}}|}{g(\mathcal{C}(\tau))} \right\}.$$

This result is obtained directly form the Euler-Lagrange equation of (11). It leads to an upper bound over the maximum curvature magnitude along the geodesics, given by

$$|\kappa| \leq \sup_{p\in[0,a]\times[0,b]} \left\{ \frac{|\nabla g(I(p))|}{g(I(p))} \right\},$$

which does not require the geodesic itself for limiting the curvature values. In [14] this bound helped in the construction of different potential functions.

A straightforward generalization of this result to our three dimensional model yields the bound over the mean curvature $\mathbf{H}$. From the equations above, it is clear that for a steady state (*i.e.* $\mathcal{S}_t = 0$) the mean curvature along the surface $\mathcal{S}$ is given by

$$\mathbf{H} = \frac{\nabla g \cdot \vec{\mathcal{N}}}{g} - \nu.$$

We readily obtain the following upper bound for the mean curvature magnitude along the final surface

$$|\mathbf{H}| \leq \sup \left\{ \frac{|\nabla g|}{g} \right\} + |\nu|,$$

where the sup operation is taken over all the $3D$ domain. The above bound gives an estimation of the allowed gaps in the edges of the object to be detected as a function of ν. A pure gap is defined as a part of the object boundary at which, for some reason, $g =$constant$\neq 0$ at a large enough neighborhood. At these locations $|\mathbf{H}| = |\nu|$. Therefore, pure gaps of radius larger than $1/\nu$ will cause the propagating surface to penetrate into the segmented object. It is also clear that $\nu = 0$, allows the detection of gaps of any given size, and the boundary at such places will be detected as the minimal surface 'gluing' the gaps boundaries.

5 Existence and uniqueness results for the minimal surfaces model

As shown in the previous section, our 3D object detection model is given by

$$u_t = g(I)|\nabla u| \left(\operatorname{div} \left(\frac{\nabla u}{|\nabla u|} \right) + \nu \right) + \nabla g \cdot \nabla u \qquad (t,x) \in [0,\infty[\times \mathbb{R}^3, \tag{24}$$

with initial condition $u(0,x) = u_0(x)$, and [8]

$$g(I) = \frac{1}{1 + |\nabla G_\sigma * I|^2}$$

with $\nu > 0$ representing a constant force in the normal direction to the level sets of u, I is the original image where we are looking for the contour of an object O, $G_\sigma * I$ is the regularized version of it by convolution with a Gaussian G_σ of variance σ. [9] $u_0(x)$ is the initial condition, usually taken as a regularized version of $1 - \chi_C$ where χ_C is the characteristic function of a set C containing O, in the case of outer deforming models (surfaces evolving towards the objects' boundary ∂O from the exterior of O), or a regularized version of χ_C where C is a set in the interior of O in the case of inner deforming models (surfaces evolving towards ∂O, starting from the inner side of O). Only the case of 2D outer snakes was considered in [6]. But it seems natural in some applications to consider the case of inner snakes [7].

Model (24) should be solved in $R = [0,1]^3$ with Neumann boundary conditions. To simplify the presentation, and as is usual done in the literature we extend the images by reflection to $\mathbb{R}^3$ and we look for solutions of (24) which are periodic, i.e., satisfying $u(t, x + 2h) = u(t,x)$ for all $x \in \mathbb{R}^3$ and $h \in \mathbb{Z}$. The initial condition $u_0(x)$ and $g(x)$ are taken extended to $\mathbb{R}^3$ with the same periodicity as u.

Existence and uniqueness results for equation (24) can be proved using the theory of viscosity solutions [15]. First we rewrite equation (24) in the form

$$\frac{\partial u}{\partial t} - g(x) a_{ij}(\nabla u)\partial_{ij} u - \nu g(x)|\nabla u| - \nabla g \cdot \nabla u = 0 \qquad (t,x) \in [0,\infty[\times \mathbb{R}^3, \tag{25}$$

where $a_{ij}(p) = \delta_{ij} - \frac{p_i p_j}{|p|^2}$ if $p \neq 0$. We use the usual notations $\partial_i u = \frac{\partial u}{\partial x_i}$, $\partial_{ij} u = \frac{\partial^2 u}{\partial x_i \partial x_j}$ and the classical Einstein summation convention in (25) and in all what follows.

Let us recall the definition of viscosity solutions. Let $u \in C([0,T] \times \mathbb{R}^3)$ for some $T \in]0,\infty[$. We say that u is a viscosity subsolution of (24) if for any function $\phi \in C^2(\mathbb{R} \times \mathbb{R}^3)$ and any local maximum $(t_0, x_0) \in]0.T] \times \mathbb{R}^3$ of $u - \phi$ we have: if $\nabla\phi(t_0,x_0) \neq 0$, then

$$\frac{\partial \phi}{\partial t}(t_0,x_0) - g(x_0) a_{ij}(\nabla\phi(t_0,x_0))\partial_{ij}\phi(t_0,x_0) - \nu g(x)|\nabla\phi(t_0,x_0)| - \nabla g(x_0) \cdot \nabla\phi(t_0,x_0) \leq 0$$

and if $\nabla\phi(t_0,x_0) = 0$, then

$$\frac{\partial \phi}{\partial t}(t_0,x_0) - g(x_0) \limsup_{p \to 0} a_{ij}(p)\partial_{ij}\phi(t_0,x_0) \leq 0$$

and $u(0,x) \leq u_0(x)$ for all $x \in \mathbb{R}^3$. In the same way we define the notion of viscosity supersolution changing "local maximum" by "local minimum", "≤ 0" by "≥ 0" and "lim sup" by "lim inf" in the expressions above. A viscosity solution is a function which is a viscosity subsolution and a viscosity supersolution.

The existence result in [6, 7] can be easily adapted to the 3D case and we recall them without proof.

[8] A specific g function is selected for the analysis, while as explained before, the model is general.

[9] Once again, the Gaussian is just an example of smoothing operator used for the analysis.

Theorem 1 *Let $W^{1,\infty}$ denote the space of bounded Lipschitz functions in $I\!R^3$. Assume that $g \geq 0$ is such that $sup\{|\nabla g^{\frac{1}{2}}(x)| : x \in I\!R^3\} < \infty$ and $sup\{|\partial_{ij} g(x)| : x \in I\!R^3, i,j = \{1,2,3\}\} < \infty$. Let $u_0, v_0 \in C(I\!R^3) \cap W^{1,\infty}(I\!R^3)$. Then*

1. *The equation (24) admits a unique viscosity solution $u \in C([0,\infty[\times I\!R^3) \cap L^\infty(0,T;W^{1,\infty}(I\!R^3))$ for all $T < \infty$. Moreover, it satisfies*

$$\inf_{I\!R^3} u_0 \leq u(t,x) \leq \sup_{I\!R^3} u_0.$$

2. *Let $v \in C([0,\infty[\times I\!R^3)$ be the viscosity solution of (2.1) with initial data v_0. Then for all $T \in [0,\infty[$ we have*

$$\sup_{0 \leq t \leq T} \| u(t,x) - v(t,x) \|_{L^\infty(I\!R^3)} \leq \| u_0(x) - v_0(x) \|_{L^\infty(I\!R^3)},$$

which means that the solution is stable.

The assumptions of Theorem (1) are just technical. They imply the smoothness of the coefficients of (25), required to prove the result using the method in [3], [6]. In particular, Lipschitz continuity in x is required. This implies a well defined trajectory of the flow $X_t = \nabla g(X)$, passing through any point $X_0 \in I\!R^3$, which is reasonable in our context. The proof of this Theorem follows the same steps of the corresponding proofs for the model (3) (see [6], Theorem 3.1), and we shall omit the details (see also [3]).

In the next Theorem, we recall a result on the independence of the generalized evolution with respect to the embedding function u_0.

Theorem 2 *Let $u_0 \in W^{1,\infty}(I\!R^3) \cap BUC(I\!R^3)$. Let $u(t,x)$ be the solution of Equation (25) as in the previous Theorem. Let $\Gamma_t := \{x : u(t,x) = 0\}$ and $D_t := \{x : u(t,x) \geq 0\}$. Then (Γ_t, D_t) are uniquely determined by (Γ_0, D_0).*

This theorem is adapted from [9], where a slightly different formulation is given. The techniques there can be applied to the present model.

Let us present some further remarks on the proposed flows (22), (23), as well as the previous geometric model (3). First note that these equations are invariant under increasing re-arrangements of contrast (morphology invariance [2]). This means that $\Theta(u)$ is a viscosity solution of the flow if u and $\Theta : I\!R \to I\!R$ are increasing functions. On the other hand, while (22) is also contrast invariant, i.e., invariant to the transformation $u \leftarrow -u$, Equations (3) and (23) are not, due to the presence of the constant velocity term $\nu g(I)|\nabla u|$. This has a double effect. First, for Equation (22), it can be shown that the generalized evolution of the level sets Γ_t only depends on Γ_0 ([18], Theorem 2.8), while for (23), the result in Theorem 2 is given. Second, for equation (22) one can show that if a smooth classical solution of the weighted minimal surface flow with $\nu = 0$ exists and is unique, then it coincides with the generalized solution obtained via the level-sets representation (22) during the lifetime of existence of the classical solution ([18], Theorem 6.1). The same result can then be proved for the general minimal surface flow ($\nu \neq 0$) and its level set representation (23), although a more delicate proof, on the lines of Corollary 11.2 in [51], is required.

Next result will be needed in the following Section to study the asymptotic behavior of the minimal surfaces model (24). Since the proof is an easy adaptation of the one in [9] (Theorem 3.2), we shall omit it as well.

Theorem 3 *Assume $S = \{x \in [0,1]^3 : g(x) = 0\}$ is a smooth compact surface, $g \geq 0$ and $\nabla g(x) = 0$ for all $x \in S$, and assume that $u_0(x) \in W^{1,\infty}(\mathbb{R}^3)$ is periodic with fundamental domain $[0,1]^3$, vanishing in an open neighborhood of S. Let $u(t,x)$ be the viscosity solution of the minimal surfaces flow. Then*

$$u(t,x) = 0 \qquad \forall x \in S, \quad \forall t \geq 0.$$

6 Correctness of the geometric minimal surfaces model

By correctness we mean the consistency of the results with our initial purpose of object detection, in an ideal case. A smooth surface in an ideal image with no noise should be recovered by our model. In this section we deal with this point.

To study the asymptotic behavior of the equation

$$u_t = g(x)|\nabla u| \left(div\left(\frac{\nabla u}{|\nabla u|}\right) + \nu\right) + \nabla g \cdot \nabla u \qquad (t,x) \in [0,\infty[\times \mathbb{R}^3 \tag{26}$$

with initial condition

$$u(0,x) = u_0(x), \qquad \forall x \in \mathbb{R}^3,$$

we assume that $S = \{x \in [0,1]^3 : g(x) = 0\}$ is a compact surface of class C^2. S divides the cube $[0,1]^3$ in two regions: the interior region and the exterior region of S. Denote these regions by $I(S)$ and $E(S)$, respectively. Observe that the interior $I(S)$ may have several connected components and $I(S)$ describes all of them together. The initial datum u_0 will be always taken in $C^2(\mathbb{R}^3)$ periodic with fundamental domain $[0,1]^3$ and vanishing in an open neighborhood of $S \cup I(S)$. Moreover, we take $u_0(x)$ such that its level sets have uniformly bounded curvatures. Let $u(t,x)$ be the unique viscosity solution of (26) given by Theorem 1 above. We follow the evolution of the set $G(t) = \{x \in [0,1]^3 : u(t,x) = 0\}$ whose boundary $S(t)$ we are interested in.

Before going into the details let us recall some elementary notions of differential geometry required below. A surface of *genus* p is a surface obtained by removing the interiors of $2p$ disjoint disks from the sphere S^2 and attaching p disjoint cylinders to their boundaries. We define the Euler-Poincare Characteristic of a surface S as $\chi(S) = 2-2p$ where p is its genus. We say that a surface S such that $\chi(S) = 2-2p$ is *unknotted* if every diffeomorphism from S to a standard p-torus can be extended to a diffeomorphism of$\mathbb{R}^3$.

We can assume that $g \geq 0$ and $\nabla g = 0, \ \ \forall x \in S$. Then, for some function $h \geq 0$ we have $g(x) = h(x)^2$ and the equation (26) in the form

$$u_t = h(x)\left(h(x)|\nabla u|\Big(div\left(\frac{\nabla u}{|\nabla u|}\right) + \nu\Big) + 2\nabla h \cdot \nabla u\right). \tag{27}$$

With this formulation, $S = \{x \in [0,1]^3 : h(x) = 0\}$.

In this section we are going to prove the following:

Theorem 4 *Assume $S = \{x \in [0,1]^3 : g(x) = 0\}$ is diffeomorphic to a sphere, i.e. $\chi(S) = 2$. If the constant ν is sufficiently large, then $S(t)$ converges to S in the Hausdorff distance as $t \to \infty$.*

Theorem 5 *Assume $S = \{x \in [0,1]^3 : g(x) = 0\}$ is diffeomorphic to a p-torus, i.e., $\chi(S) = 2 - 2p$ and is unknotted. If ν is sufficiently large, then $S(t)$ converges to S in the Hausdorff distance as $t \to \infty$.*

Theorem 6 *Assume $S = \{x \in [0,1]^3 : g(x) = 0\}$ is the knotted surface of Figure 5. If ν is sufficiently large, then $S(t)$ converges to S in the Hausdorff distance as $t \to \infty$.*

Proof of Theorem 4

The proof is based on Lemma 1 and Lemma 2 below.

Lemma 1 *$I(S) \subset \{x \in [0,1]^3 : u(t,x) = 0\}$ for all $t > 0$*

Proof: In Theorem 3 we proved that $u(t,x) = 0$ for all $x \in S$ and all $t > 0$. Consider the problem

$$\begin{array}{ll} z_t = g(x)|\nabla z| \left(div \left(\frac{\nabla z}{|\nabla z|} \right) + \nu \right) + \nabla g \cdot \nabla u & (t,x) \in [0,\infty[\times I(S) \\ z(0,x) = u_0(x) \quad x \in I(S) & \\ z(t,x) = 0 \quad x \in S \quad t \geq 0 & \end{array} \tag{28}$$

We know that $z(t,x) = 0$ and $z(t,x) = u(t,x)$ are two viscosity solutions of (28). Since there is uniqueness of viscosity solutions of this problem, it follows that $u(t,x) = 0$ for all $(t,x) \in [0,\infty] \times I(S)$. $\square$

Remark: Lemma 1 is also true if S is as in Theorem 5.

Lemma 2 *Assume $S = \{x \in [0,1]^3 : g(x) = 0\}$ is diffeomorphic to a sphere, i.e., $\chi(S) = 2$. If the constant ν is sufficiently large, for any $\eta > 0$, there exists some $T_\eta > 0$ such that*

$$G(t) \subset \{x \in [0,1]^3 : d(x, I(S)) < 2\eta\}$$

for all $t > T_\eta$.

Proof: Essentially, the proof of this lemma consists in constructing a subsolution of (26) which becomes strictly positive as $t \to \infty$. If S is a convex C^2 surface this is not a difficult task. In this case the distance function to S, $d(x) = d(x,S)$, $x \in E(S)$ is of class C^2 in $E(S)$. This function is the tool to construct the desired subsolution. In the general case S needs not be convex and the proof is a bit more technical and we need a geometric construction.

Let S_1 be a compact surface of class C^2 contained in $\{x \in [0,1]^3 : u_0(x) > 0\} \cap E(S)$. Consider $E = \{x \in [0,1]^3 : x \in I(S_1) \cap E(S)\}$. E is diffeomorphic to the closed annulus $A = \{x \in \mathbb{R}^3 : r' \leq |x| \leq r"\}$. There is a C^2 diffeomorphism ϕ between A and E. Consider the family ζ_r of surfaces

$$\zeta_r(\theta,\varphi) = (r\cos\theta\cos\varphi, r\cos\theta\sin\varphi, r\sin\theta) \qquad r' \leq r \leq r", \ -\frac{\pi}{2} < \theta \leq \frac{\pi}{2}, \ 0 \leq \varphi < 2\pi.$$

This family is mapped by ϕ into a family of surfaces $S(r)$ in E of class C^2, i.e. $S(r) = \phi \circ \zeta_r$. Without loss of generality we may suppose that $\Gamma(r') = S$ and $\Gamma(r") = S_1$. Since the surfaces $\zeta_r \quad r' \leq r \leq r"$ have uniformly bounded curvatures it follows that the family of surfaces $S(r), \quad r' \leq r \leq r"$ have uniformly bounded curvatures.

We may choose $\rho > 0$ such that we have $\nabla h \cdot \nabla d(x, S) > 0$ on $E(S) \cap (S + B(0, \rho))$.

For any $\eta > 0$, we can take $n = n(\eta)$ and $r" = r_1 > r_2 > \cdots > r_n$ sufficiently close to each other and r_n near to r' such that the family of surfaces $S_i = \phi \circ \zeta_{r_i}$ satisfies the following:

1. $S_i \in C^2$ with interior region $I(S_i)$ and exterior region $E(S_i)$, $i = 1, \ldots, n$, and with $S_i \subset I(S_{i-1})$, $i = 2, \ldots, n$.

2. $S_1 \subset \{x \in [0,1]^3 : u_0(x) > 0\}$ and $S_n \subset \{x \in E(S) : 0 < d(x, S) < \eta\}$.

3. For each $x \in S_i$, let $k_i^j(x) \quad j = 1, 2$ the principal curvatures of S_i at the point x. Let $K_i = max\{|k_i^j(x)| : x \in S_i, \; j = 1, 2\}$. We suppose (to ensure regularity) that $S_i \subset \{x \in E(S_{i+1}) : d(x, S_{i+1}) < \frac{1}{2K_{i+1}}\}$

4. $\sup\{K_i, i = 1, \ldots, n\} \leq M$ with a constant M independent of η.

From these surfaces we construct another family S_i^* such that, $S_1^* = S_1$ and for each $i = 2, \ldots, n-1$, let S_i^* be a regular surface contained in $\{x \in E(S_i) \cap I(S_{i-1}) : d(x, S_i) < \frac{1}{4K_{i+1}}\}$. Finally, let S_n^* be a smooth surface contained in $\{x \in E(S_n) \cap I(S_{n-1}) : d(x, S) < 2\eta\}$. Each surface S_i^* is in a neighborhood of S_{i+1} of radius $\frac{3}{4K_{i+1}}$.

Let R_i be the region between the surfaces S_{i-1}^* and S_i, $i = 2, \ldots, n$ (see Figure 2). Let $d_i(x) = d(x, S_i)$ for $x \in R_i$, and let $C_i > 0$ be a constant such that $d_i(x) \leq C_i h(x)$ for $x \in R_i$, $i = 2, \ldots, n$. Notice also that we are working in the unit cube and $d_i(x) \leq \sqrt{3}$. We may also suppose that there exists $n' < n$ such that for $i \geq n'$ we have $R_i \subset E(S) \cap (S + B(0, \rho))$. Since assuming that $\nabla h \cdot \nabla d(x, S) > 0$, by continuity we may choose ρ small enough such that when $i \geq n'$ we have $\nabla h \cdot \nabla d_i \geq 0$.

Our purpose is to construct a family of subsolutions, which becomes asymptotically positive as $t \to \infty$ on each R_i. By the last of our assumptions on u_0, we may choose a constant ν in (27) sufficiently large independent of the geometric construction such that for some $\delta > 0$

$$\Delta d_i + \nu \geq \delta > 0 \qquad \text{in} \quad R_i \quad i = 2, \ldots, n \tag{29}$$

and u_0 is a subsolution of the (27), i.e.

$$|\nabla u_0| h(x) \left(div \left(\frac{\nabla u_0}{|\nabla u_0|} \right) + \nu \right) + 2\nabla h \cdot \nabla u_0 \geq 0. \tag{30}$$

Remark: If $i \leq n' - 1$ we take ν large enough such that $\delta > \frac{2C}{\inf_{E(S)\cap(S+B(0,\rho))} h}$ where C is an upper bound for $|\nabla h \cdot \nabla d_i|$, $i = 2, \cdots n' - 1$. With this we obtain that for some $\delta_1 > 0$,

$$h(x)(\Delta d_i + \nu) + 2\nabla h \cdot \nabla d_i \geq \delta_1 > 0 \qquad x \in R_i, \quad i = 2, \cdots n' - 1.$$

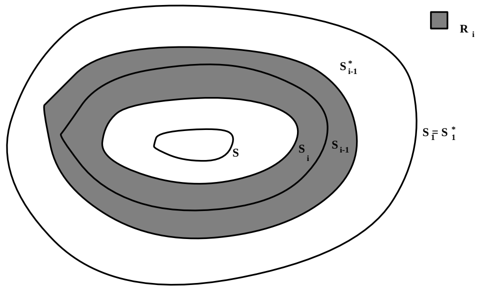

Figure 2: Construction for Lemma 2.

If $i \geq n'$ we have $R_i \subset E(S) \cap (S + B(0, \rho))$, and $Dh \cdot Dd_i > 0$. In this case, we also obtain that, for some $\delta_2 > 0$,

$$h(x)(\Delta d_i + \nu) + 2\nabla h \cdot \nabla d_i \geq \delta_2 > 0 \qquad i \geq n'$$

On each region R_i we consider the problem:

$$\begin{array}{l} z_t = g(x)|\nabla z| \left(div \left(\frac{\nabla z}{|\nabla z|} \right) + \nu \right) + \nabla g \cdot \nabla z \qquad (t,x) \in [T_{i-1}, \infty[\times R_i \\ z(t,x) = 0 \qquad x \in S_i \qquad t \in [T_{i-1}, \infty[\\ z(t,x) = u(t,x) \qquad x \in S^*_{i-1} \qquad t \in [T_{i-1}, \infty[\\ z(T_{i-1}, x) = 0 \qquad x \in R_i \end{array} \tag{31}$$

where T_i will be specified later. We want to construct a family of subsolutions of (31) which becomes positive as $t \to \infty$. Obviously $u(t,x)$, the viscosity solution of (26) given by Theorem 1, is a supersolution of the problem (31), and by (30) u_0 is a subsolution of (26). We shall use the following comparison principle [15]

Theorem 7 *Let $w, v \in C([0, \infty[, C(R_i))$ be respectively a bounded sub and supersolution of (31). Then $w(t,x) \leq v(t,x)$ for all $(t,x) \in [0, \infty[\times R_i$. The same comparison holds for (26).*

The previous result implies $u(t,x) \geq u_0(x)$ for all $(t,x) \in [0, \infty[\times I\!\!R^3$. In particular we have

$$\inf\{u(t,x) : t \in [0, \infty[, x \in E(S^*_1)\} \geq inf\{u_0(x), x \in E(S^*_1)\} > 0. \tag{32}$$

Assume we have shown that for all $j < i$ there exists some T_j such that

$$\inf\{u(t,x) : t \in [T_j, \infty[, \quad x \in E(S^*_j)\} \geq \beta_j > 0. \tag{33}$$

By (32) this is true when $i = 2$ with $T_1 = 0$.

For constructing the subsolution of (31) in $[T_{i-1},\infty[\times R_i$, $i=2,\dots,n$ we change variables and take $T_{i-1}=0$. Let

$$w_m(t,x) = f_m(t)d_i(x) + g_m(t), \tag{34}$$

where $(t,x)\in[0,\infty[\times R_i, \quad m>0$

$$f_m(t) = \lambda(1-\frac{1}{(1+t)^m}) \qquad \lambda>0 \tag{35}$$

$$g_m(t) = g_m t \qquad t\in[0,t_m] \qquad g_m(t) = g_m t_m \qquad t>t_m, \tag{36}$$

where $g_m = -2m\lambda$ and $t_m = (1+\frac{mC_i}{\delta_0})^{\frac{1}{m}} - 1$ where $\delta_0 = \min(\delta_1,\delta_2)$. With these functions we have

Lemma 3 *For $\lambda>0$ small enough and for all $m>0$, w_m is a subsolution of (31).*

Proof: It is clear by construction that $w_m(t,x)\le 0$ for $(t,x)\in[T_{i-1},\infty[\times S_i$ and $w_m(T_{i-1},x)\le 0$ for $x\in R_i$.

Using (33), taking $\lambda>0$ sufficiently small, we have $w_m(t,x)\le u(t,x)$ for $(t,x)\in[T_{i-1},\infty[\times S^*_{i-1}$.

The function w_m has been chosen such that

$$\frac{\partial w_m}{\partial t} - h(x)\left(h(x)|\nabla w_m|\Big(div\left(\frac{\nabla w_m}{|\nabla w_m|}\right)+\nu\Big) + 2Dh\cdot\nabla w_m\right) \le 0 \qquad \text{in} \quad [0,\infty[\times R_i. \tag{37}$$

Indeed, if $t<t_m$ we have

$$f'_m(t)d_i(x) + g'_m(t) - h(x)f_m(t)(h(x)(\Delta d_i+\nu) + 2\nabla h\cdot\nabla d_i \le$$

$$\le f'_m(t)d_i(x) + g_m \le f'_m(0)d_i(x) + g_m \le \sqrt{3}\lambda m + g_m \le q0.$$

If $t>t_m$ we have

$$f'_m(t)d_i(x) - h(x)f_m(t)(h(x)(\Delta d_i+\nu) + 2\nabla h\cdot\nabla d_i \le$$

$$\le f'_m(t)C_ih(x) - h(x)f'_m(t)\delta_0 \le f'_m(t_m)C_ih(x) - h(x)f_m(t_m)\delta_0.$$

Using the expressions for t_m we immediately see that the last expression is ≤ 0. This completes the proof of the lemma. □

Lemma 4 *$u(t,x)\ge w_m(t,x)$ for all $(t,x)\in[T_{i-1},\infty[\times R_i$. Hence, there exist $m_0>0$ and $T_i>0$ such that*

$$u(t,x) \ge \inf\{w_m(t,x) : t\in[T_{i-1},\infty[,\ x\in R_i\cap E(S^*_i)\} > 0$$

for all $t\in[T_{i-1},\infty[$, $x\in R_i\cap E(S^*_i)$ and all $m<m_0$.

Proof: The first inequality follows from Lemma 3 and Theorem 7. On the other hand we observe that

$$w_m(t,x) \to \lambda d_i(x) + g_m t_m \qquad as \qquad t \to \infty. \tag{38}$$

Since t_m is bounded and $g_m \to 0$ as $m \to 0$, there exists some $m_0 > 0$ such that

$$\inf\{\lambda d_i(x) + g_m t_m : x \in R_i \cap E(S_i^*)\} > 0 \tag{39}$$

for all $0 < m < m_0$. The lemma follows from (38) and (39). □

Lemma 4 is a consequence of the last two lemmas.

Remark: If we consider the model (27) with $\nu = 0$, i.e.,

$$u_t = g(x)|\nabla u| div\left(\frac{\nabla u}{|\nabla u|}\right) + \nabla g(x) \cdot \nabla u \tag{40}$$

with $g(x) = h^2(x)$ as above, a theorem similar to Theorem 4 above holds if we take our initial surface sufficiently close to S. For that, we consider (40) on $[0, +\infty[\times V$ where V is a neighborhood of $I(S)$ together with initial and boundary conditions

$$\begin{aligned} u(0,x) &= u_0(x) \qquad x \in V \\ u(t,x) &= u_0(x) \qquad t > 0 \quad x \in \partial V \end{aligned}$$

Moreover, V should be taken sufficiently near to S, i.e., $V \subset I(S) + B(0,\rho)$ for ρ small enough, so that

$$h(x)\Delta d(x) + 2\nabla h(x) \cdot \nabla d(x) \geq 0 \qquad x \in V - \overline{I(S)},$$

where $d(x) = d(x,S)$. In that case, we can adapt the ideas above to prove that $S(t) = \partial\{x : u(t,x) = 0\} \to S$ as $t \to \infty$.

Proof of Theorem 5

Lemma 5 *Suppose that $S = \{x \in [0,1]^3 : g(x) = 0\}$ is diffeomorphic to a p-torus, i.e., $\chi(S) = 2 - 2p$ and is unknotted. If ν is sufficiently large, for any $\eta > 0$ there exist some $T_\eta > 0$ such that*

$$G(t) \subset \{x \in [0,1]^3 : d(x, I(S)) < \eta\} \qquad t > T_\eta.$$

Proof: The idea of the proof is to construct two surfaces Γ_1 and Γ_2 of class C^2 and diffeomorphic to a sphere, i.e. $\chi(\Gamma_i) = 2$, $i = 1,2$, such that the boundary of $I(\Gamma_1) \cap I(\Gamma_2)$ is diffeomorphic to a p-torus and near S. We prove that for a large t, $S(t)$ is near the boundary of $I(\Gamma_1) \cap I(\Gamma_2)$, therefore $S(t)$ will be near S. Let us, first of all, construct the surfaces Γ_1 and Γ_2.

Given $\eta > 0$ we choose Γ_1 and Γ_2 satisfying:

1. Γ_i is a compact surface of class C^2, $\chi(\Gamma_i) = 2$ and $I(S) \subset I(\Gamma_i)$ $\ i = 1,2$.

2. $U_\eta := [I(\Gamma_1) + B(0, \frac{\eta}{2})] \cap [I(\Gamma_2) + B(0, \frac{\eta}{2})]$ is an open set whose boundary is a regular surface diffeomorphic to a p-torus.

3. $U_\eta \subset I(S) + B(0, \eta)$

Recall that the sum of two sets A, B is defined by $A + B = \{a + b : a \in A, b \in B\}$

If S is a standard p-torus, which we denote by T_p, it is easy to construct surfaces Γ_1 and Γ_2 satisfying the conditions above. Since this is technically delicate, but easy to see graphically, we illustrate it in Figure 3.

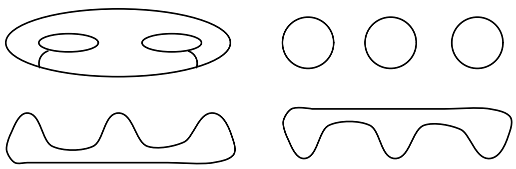

Figure 3: Construction of Γ_1 and Γ_2 for Lemma 5.

If S is not a standard p-torus, then (see [16], Chapter 4) it is diffeomorphic to a standard p-torus and there exists a diffeomorphism $f : S \to T_p$. As S is unknotted this diffeomorphism can be extended to all $I\!R^3$ $F : I\!R^3 \to I\!R^3$ such that $F|_S = f$. In this case we construct the surfaces $\widetilde{\Gamma_1}$ and $\widetilde{\Gamma_2}$ as $\widetilde{\Gamma_i} = F^{-1}(\Gamma_i)$, $\;i = 1, 2$. They also satisfy the above conditions.

By Theorem 4, we know that for ν sufficiently large there exists $T^i_\eta > 0$ such that $G(t) \subset \{x \in [0,1]^3 : d(x, I(\Gamma_i)) < \frac{\eta}{2}\}$ for all $t > T^i_\eta$, $i = 1, 2$. Then, we choose $T_\eta = max(T^1_\eta, T^2_\eta)$ and we have

$$G(t) \subset [I(\Gamma_1) + B(0, \frac{\eta}{2})] \cap [I(\Gamma_2) + B(0, \frac{\eta}{2})], \quad t > T_\eta.$$

Hence $G(t) \subset U_\eta \subset I(S) + B(0, \eta)$ for all $t > T_\eta$.□

Remark: From the proof above, it is easy to see that if S_1, S_2 are two surfaces for which the condition: " for any $\eta > 0$ there exist some $T_\eta > 0$ such that $G(t) \subset \{x \in [0,1]^3 : d(x, I(S_i)) < \eta\}$ $\;i = 1, 2$ for $t > T_\eta$," is true, then it is also true for $S_1 \cap S_2$.

Using this remark, one can prove that if $S = \{x \in [0,1]^3 : g(x) = 0\}$ is the knotted surface of Figure 5, then for any $\eta > 0$ there exist some $T_\eta > 0$ such that

$$G(t) \subset \{x \in [0,1]^3 : d(x, I(S)) < \eta\} \quad t > T_\eta.$$

For the proof, we consider two unknotted surfaces diffeomorphics to a p-torus such that their intersection is the knotted surface and use the remark above conclude the proof. How do we construct such surfaces? First of all, observe that by attaching a finite number of thin cylinders (which can be done in a smooth way) we can get a smooth surface diffeomorphic to a p-torus for some $p \in I\!N$. This can be done in two different ways Γ_1, Γ_2 such that the boundary of $I(\Gamma_1) \cap I(\Gamma_2)$ is diffeomorphic to the knotted surface of Figure 5 and near to it. Of course such result can be proven for all knotted surfaces where the above strategy can be used.

Remark: If $u_0(x)$ is taken as

$$u_0(x) = \begin{cases} > 0 & \text{if } x \in \overline{B(y,r)} \subset I(S) \\ 0 & \text{if } x \text{ in a neigborhood of } S \cup E(S)\,, \end{cases}$$

i.e., a function vanishing in a neighborhood of $S \cup E(S)$, and such that its levels sets have uniformly bounded curvatures, then we may recover a surface S starting from its inner region. The proof of this result is similar to the proof of Theorem 4. Lemma 1 and Lemma 2 are essentially the same except of replacing $I(S)$ by $E(S)$. Hence, we shall omit the details.

7 Experimental results

We now present some examples of our minimal surfaces deformable model (15). The numerical implementation is based on the algorithm for surface evolution via level sets developed by Osher and Sethian [40, 54] and recently used by many authors for different problems in computer vision and image processing. The algorithm allows the evolving surface to change topology without monitoring the deformation. This means that several objects can be detected simultaneously, although it is not required to know that there are more than one in the image. Note that when implementing our model with this algorithm, the extension of the image-based speed performed in [33, 34, 35] is not necessary. Furthermore, using new results in [1], the algorithm can be made to converge very fast. In the numerical implementation of equation (15) we have chosen central difference approximation in space and forwards difference approximation in time. This simple selection is possible due to the stable nature of the equation, however, when the coefficient ν is taken to be of high value or when the gradient term is dominant, more sophisticated approximations are required [40]. See the mentioned references for details on the numerics.

Figure 4 presents an example of the geodesic active contours from [7]. The figure on the left is the original image, and the one on the right present the evolving curves (gray) and the detected boundaries (white). The initial curves are the two small circles in the tools. Both interior and exterior boundaries are detected without any special tracking procedure.

The first example of the minimal surfaces deformable model is presented in Figure 5. This object is composed by two torus, one inside the other (knotted surface). The initial surface is an ellipsoid surrounding the two torus (top left). Note how the model manages to split and detect this very different topology (bottom right).

A medical example is given in figure 6 and 7. Figure 6 presents the 3D detection of a tumor in an MRI image. The initial 3D shape is presented in the first row. The second row presents 3 evolution steps, while the final shape, the weighted minimal surface, is presented in the bottom. Figure 7 shows slices of this 3D detection, together with the corresponding MRI data.

8 Concluding remarks

In this paper we presented a novel formulation of deformable surfaces for three dimensional object detection, extending previously reported two dimensional work [7]. We showed that

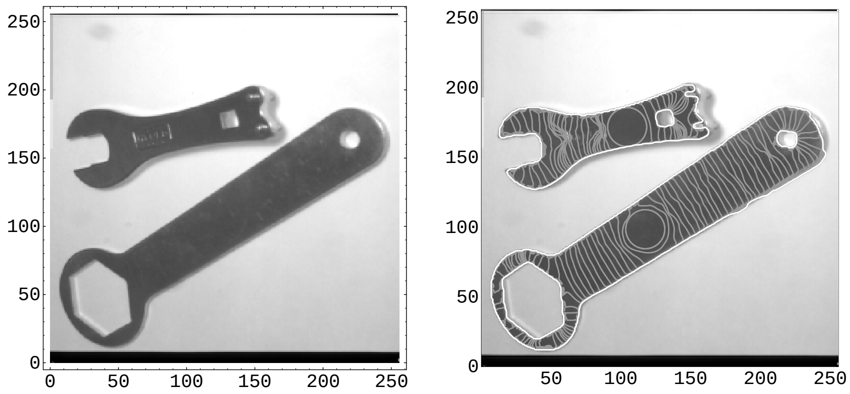

Figure 4: Example of the geodesic active contours. From the two small circles, both interior and exterior boundaries are detected without any special tracking procedure.

the solution to the deformable surfaces approach for boundary detection is given by a minimal surface in a Riemannian space defined by a metric derived from the given image. This means that detecting the object is equivalent to finding a surface of minimal weighted area. This approach allowed to relate classical energy based models with new surface evolution ones. The minimal surfaces formulation introduced a new term that attracts the deforming surface to the boundary, improving the detection of boundaries with large differences in their gradient. This new term also frees the model from the need to estimate critical parameters. Therefore, the minimal surfaces formulation not only connects previous models, but also improves them. We also presented results regarding the existence, uniqueness, stability, and correctness of the solution obtained by our model.

We presented experiments for different kind of images. These experiments showed the possibility to detect several objects, as well as the possibility to detect interior and exterior boundaries at the same time. The sub-pixel accuracy intrinsic to the algorithm allows to perform accurate measurements after the object is detected [44].

The model presented is general, as well as the approach for solving image analysis problems via geodesic or minimal surfaces computation. Other image processing and computer vision problems, like the shape from shading [28, 29, 37, 43], can be reformulated as the computation of geodesics or minimal distances as well. The metric is specified by the image and the application. We are currently investigating this geodesic/minimal-surface-type approach for other problems in image analysis.

Acknowledgments

The authors thank Prof. J. Blat, Prof. P.L. Lions, and Prof. J.M. Morel for interesting discussions and their constant support.

References

[1] D. Adalsteinsson and J. A. Sethian, “A fast level set method for propagating interfaces,” *LBL TR-University of Berkeley*, December 1993.

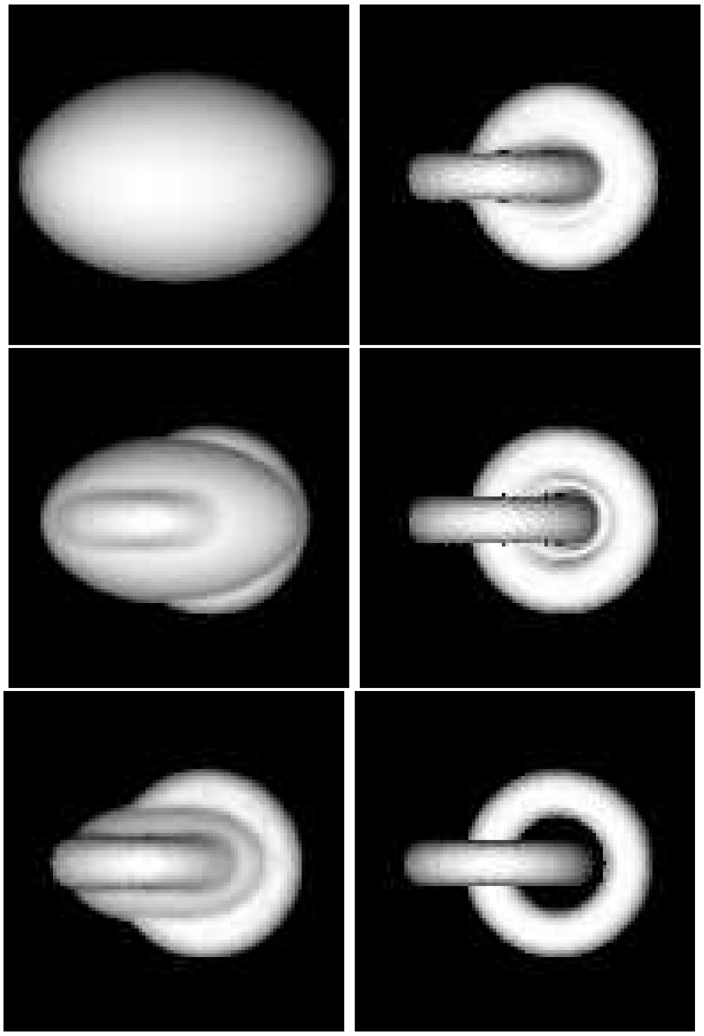

Figure 5: Detection of a linked torus.

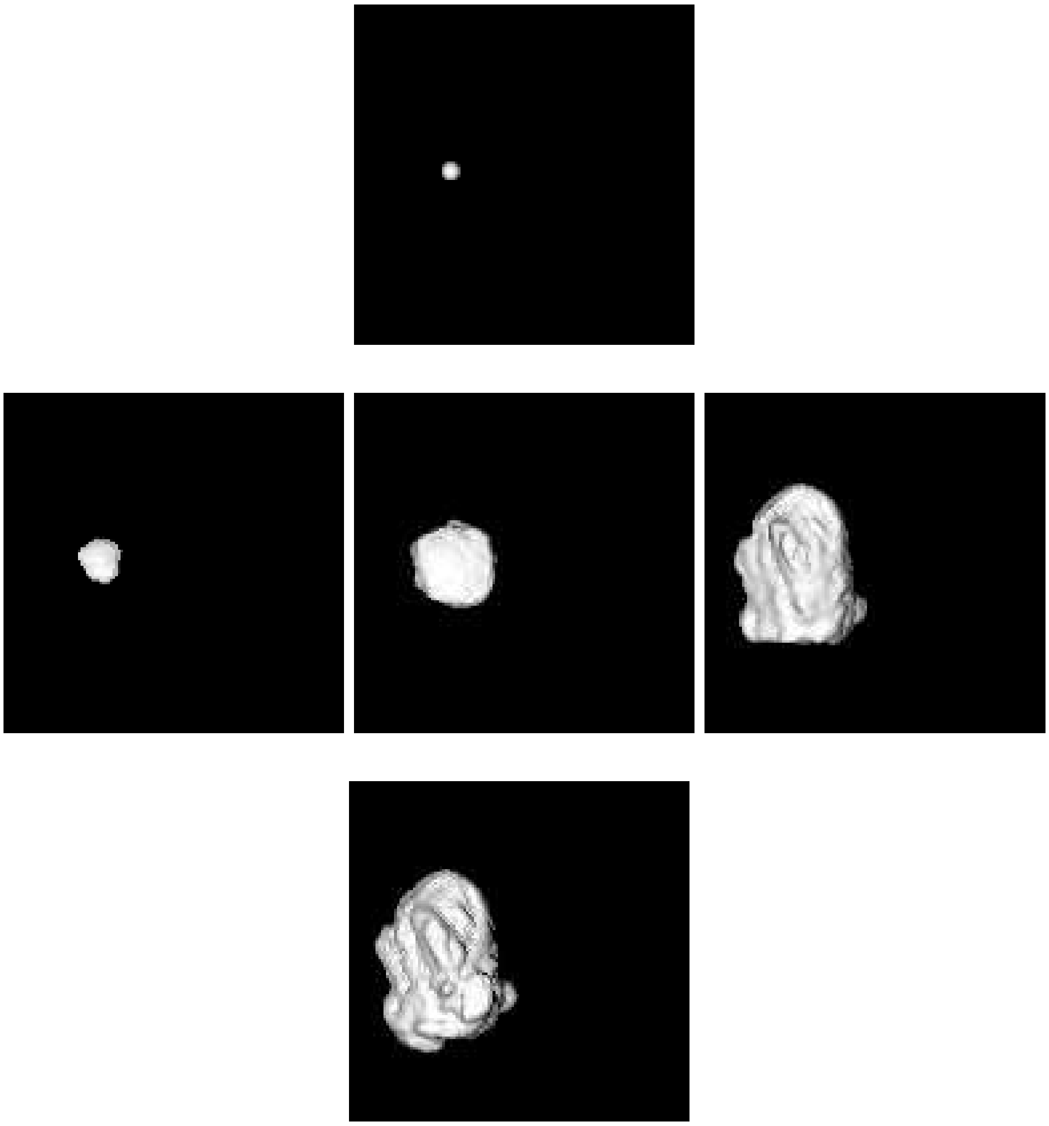

Figure 6: Detection of a tumor in MRI.

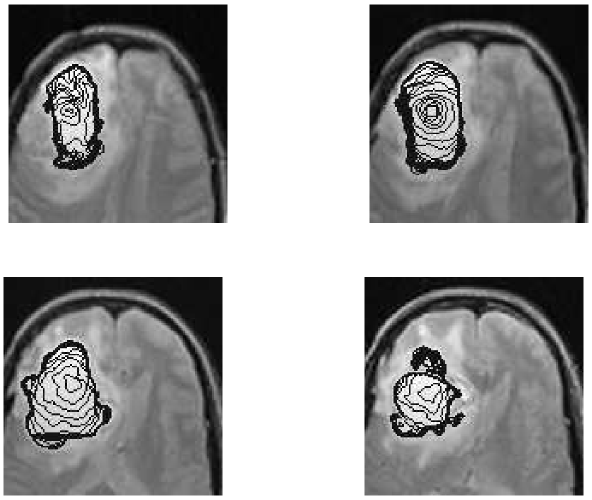

Figure 7: Slices of the 3D detection in Figure 6.

[2] L. Alvarez, F. Guichard, P. L. Lions, and J. M. Morel, "Axioms and fundamental equations of image processing," *Arch. Rational Mechanics* **123**, 1993.

[3] L. Alvarez, P. L. Lions, and J. M. Morel, "Image selective smoothing and edge detection by nonlinear diffusion," *SIAM J. Numer. Anal.* **29**, pp. 845-866, 1992.

[4] S. Angenent, "Parabolic equations for curves on surfaces, Part II. Intersections, blow-up, and generalized solutions," *Annals of Mathematics* **133**, pp. 171-215, 1991.

[5] A. Blake and A. Zisserman, *Visual Reconstruction*, MIT Press, Cambridge, 1987.

[6] V. Caselles, F. Catte, T. Coll, F. Dibos, "A geometric model for active contours," *Numerische Mathematik* **66**, pp. 1-31, 1993.

[7] V. Caselles, R. Kimmel, and G. Sapiro, "Geodesic active contours," HP Labs Technical Report, September 1994, submitted. A short version appears at *ICCV'95*, Cambridge, June 1995.

[8] V. Caselles and C. Sbert, "What is the best causal scale-space for 3D images?," *SIAM J. on Applied Math,* to appear.

[9] Y. G. Chen, Y. Giga, and S. Goto, "Uniqueness and existence of viscosity solutions of generalized mean curvature flow equations," *J. Differential Geometry* **33**, pp. 749-786, 1991.

[10] D. Chopp, "Computing minimal surfaces via level set curvature flows," *LBL TR-University of Berkeley*, 1991.

[11] P. Cinquin, "Un modele pour la representation d'images medicales 3d," *Procee. Euromedicine, Sauramps Medical*, **86**, pp 57-61, 1986.

[12] L. D. Cohen, "On active contour models and balloons," *CVGIP: Image Understanding* **53**, pp. 211-218, 1991.

[13] I. Cohen, L. D. Cohen, and N. Ayache, "Using deformable surfaces to segment 3D images and infer differential structure," *CVGIP: Image Understanding* **56**, pp. 242-263, 1992.

[14] L. D. Cohen, and R. Kimmel, "Minimal geodesics of active contour models for edge integration and segmentation," TR-INRIA, 1995.

[15] M. G. Crandall, H. Ishii, and P. L. Lions, "User's guide to viscosity solutions of second order partial linear differential equations," *Bulletin of the American Math. Society* **27**, pp. 1-67, 1992.

[16] M. P. Do Carmo, *Differential Geometry of Curves and Surfaces*, Prentice-Hall, 1976.

[17] B. A. Dubrovin, A. T. Fomenko, and S. P. Novikov, *Modern Geometry - Methods and Applications I*, Springer-Verlag, New York, 1984.

[18] L. C. Evans and J. Spruck, "Motion of level sets by mean curvature, I," *J. Differential Geometry* **33**, pp. 635-681, 1991.

[19] O. Faugeras, "On the evolution of simple curves of the real projective plane," *Comptes rendus de l'Acad. des Sciences de Paris* **317**, pp. 565-570, September 1993.

[20] M. Gage and R. S. Hamilton, "The heat equation shrinking convex plane curves," *J. Differential Geometry* **23**, pp. 69-96, 1986.

[21] M. Grayson, "The heat equation shrinks embedded plane curves to round points," *J. Differential Geometry* **26**, pp. 285-314, 1987.

[22] H. W. Guggenheimer, *Differential Geometry*, McGraw-Hill Book Company, New York, 1963.

[23] M. Kass, A. Witkin, and D. Terzopoulos, "Snakes: Active contour models," *International Journal of Computer Vision* **1**, pp. 321-331, 1988.

[24] S. Kichenassamy, A. Kumar, P.Olver, A. Tannenbaum, and A. Yezzi, "Gradient flows and geometric active contour models," *Proc. ICCV*, Cambridge, June 1995.

[25] B. B. Kimia, A. Tannenbaum, and S. W. Zucker, "Shapes, shocks, and deformations, I," *International Journal of Computer Vision*, to appear.

[26] R. Kimmel, A. M. Bruckstein, "Shape offsets via level sets, " *CAD* **25:5**, pp. 154-162, 1993.

[27] R. Kimmel, A. Amir, A. M. Bruckstein, "Finding shortest paths on surfaces using level sets propagation," *IEEE–PAMI*, to appear.

[28] R. Kimmel and A. M. Bruckstein, "Tracking level sets by level sets: A method for solving the shape from shading problem," *CVIU*, to appear.

[29] R. Kimmel, K. Siddiqi, B. B. Kimia, A. M. Bruckstein, "Shape from shading: Level set propagation and viscosity solutions," *International Journal of Computer Vision*, to appear.

[30] R. Kimmel, N. Kiryati, A. M. Bruckstein, "Distance maps and weighted distance transforms," *Journal of Mathematical Imaging and Vision,* Special Issue on Topology and Geometry in Computer Vision, to appear.

[31] R. Kimmel and G. Sapiro, "Shortening three dimensional curves via two dimensional flows," *International Journal of Computer & Mathematics with Applications* **29**, pp. 49-62, 1995.

[32] W. J. Niessen, B. M. ter Haar Romeny, L. M. J. Florack, and A. H. Salden, "Nonlinear diffusion of scalar images using well-posed differential operators," Technical Report, Utrecht University, The Netherlands, October 1993.

[33] R. Malladi, J. A. Sethian and B. C. Vemuri, "Evolutionary fronts for topology independent shape modeling and recovery," *Proc. of the 3rd ECCV*, Stockholm, Sweden, pp. 3-13, 1994.

[34] R. Malladi, J. A. Sethian and B. C. Vemuri, "Shape modeling with front propagation: A level set approach," *IEEE Trans. on PAMI,* January 1995.

[35] R. Malladi, J. A. Sethian and B. C. Vemuri, "A fast level set based algorithm for topology independent shape modeling," *Journal of Mathematical Imaging and Vision*, Special Issue on Topology and Geometry, Ed. A. Rosenfeld and Y. Kong, to appear.

[36] T. McInerney and D. Terzopoulos, "Topologically adaptable snakes," *Proc. ICCV*, Cambridge, June 1995.

[37] J. Oliensis and P. Dupuis, "Direct Method For Reconstructing Shape From Shading," *Proceedings SPIE Conf. 1570 on Geometric Methods in Computer Vision*, pp. 116-128, 1991.

[38] P. J. Olver, G. Sapiro, and A. Tannenbaum, "Differential invariant signatures and flows in computer vision: A symmetry group approach," in *Geometry Driven Diffusion in Computer Vision*, B. Romeny (Ed.), Kluwer, 1994.

[39] P. J. Olver, G. Sapiro, and A. Tannenbaum, "Invariant geometric evolutions of surfaces and volumetric smoothing," *SIAM J. of Appl. Math.*, to appear.

[40] S. J. Osher and J. A. Sethian, "Fronts propagation with curvature dependent speed: Algorithms based on Hamilton-Jacobi formulations," *Journal of Computational Physics* **79**, pp. 12-49, 1988.

[41] R. Osserman, *Survey of Minimal Surfaces*, Dover, 1986.

[42] B. Romeny, *Gometry Driven diffusion in Computer Vision*, Kluwer, 1994.

[43] E. Rouy and A. Tourin, "A viscosity solutions approach to shape-from-shading," *SIAM. J. Numer. Analysis* **29**, pp. 867-884, 1992.

[44] G. Sapiro, R. Kimmel, and V. Caselles, "Object detection and measurements in medical images via geodesic active contours," SPIE-Vision Geometry, San Diego, July 1995.

[45] G. Sapiro, R. Kimmel, D. Shaked, B. B. Kimia, and A. M. Bruckstein, "Implementing continuous-scale morphology via curve evolution," *Pattern Recog.* **26:9**, pp. 1363-1372, 1993.

[46] G. Sapiro and A. Tannenbaum, "On affine plane curve evolution," *Journal of Functional Analysis* **119:1**, pp. 79-120, 1994.

[47] G. Sapiro and A. Tannenbaum, "Affine invariant scale-space," *International Journal of Computer Vision* **11:1**, pp. 25-44, 1993.

[48] G. Sapiro and A. Tannenbaum, "On invariant curve evolution and image analysis," *Indiana University Mathematics Journal* **42:3**, 1993.

[49] G. Sapiro and A. Tannenbaum, "Area and length preserving geometric invariant scale-spaces," *IEEE Trans. PAMI* **17:1**, pp. 67-72, 1995.

[50] G. Sapiro and A. Tannenbaum, "Edge preserving geometric enhancement of MRI data," EE-TR, University of Minnesota, April 1994.

[51] H.M. Soner, "Motion of a set by the curvature of its boundary," *J. of Diff. Equations* **101**, pp. 313-372, 1993.

[52] J. Shah, "Recovery of shapes by evolution of zero-crossings," Technical Report, Math. Dept. Northeastern Univ. Boston MA, 1995.

[53] R. Szeliski, D. Tonnesen, and D. Terzopoulos, "Modeling surfaces of arbitrary topology with dynamic particles," *Proc. CVPR*, pp. 82-87, 1993.

[54] J. A. Sethian, "A review of recent numerical algorithms for hypersurfaces moving with curvature dependent flows," *J. Differential Geometry* **31**, pp. 131-161, 1989.

[55] D. Terzopoulos, A. Witkin, and M. Kass, "Constraints on deformable models: Recovering 3D shape and nonrigid motions," *Artificial Intelligence* **36**, pp. 91-123, 1988.